Photochemical route to actinide-transition metal bonds: synthesis, characterization and reactivity of a series of thorium and uranium heterobimetallic complexes

Ashleigh L. Ward,[†‡] Wayne W. Lukens,[‡] Connie C. Lu,[*§] and John Arnold[*†‡]

[†]Department of Chemistry, University of California, Berkeley, California 94720, United States

[‡]Chemical Sciences Division, Lawrence Berkeley National Lab, Berkeley, California 94720, United States

[§]Department of Chemistry, University of Minnesota, Minneapolis, Minnesota 55455, United States

Supporting Information Placeholder

ABSTRACT: A series of actinide-transition metal heterobimetallics has been prepared, featuring thorium, uranium and cobalt. Complexes incorporating the binucleating ligand N[*o*-(NHCH$_2$P^{i}Pr$_2$)C$_6$H$_4$]$_3$ and Th(IV) (**4**) or U(IV) (**5**) with a carbonyl bridged [Co(CO)$_4$]$^-$ unit were synthesized from the corresponding actinide chlorides (Th: **2**; U: **3**) and Na[Co(CO)$_4$]. Irradiation of the isocarbonyls with ultraviolet light resulted in the formation of new species containing actinide-metal bonds in good yields (Th: **6**; U: **7**); this photolysis method provides a new approach to a relatively rare class of complexes. Characterization by single-crystal X-ray diffraction revealed that elimination of the bridging carbonyl is accompanied by coordination of a phosphine arm from the N$_4$P$_3$ ligand to the cobalt center. Additionally, actinide-cobalt bonds of 3.0771(5) Å and 3.0319(7) Å for the thorium and uranium complexes, respectively, were observed. The solution state behavior of the thorium complexes was evaluated using ^{1}H, ^{1}H-^{1}H COSY, ^{31}P and variable-temperature NMR spectroscopy. IR, UV-Vis/NIR, and variable-temperature magnetic susceptibility measurements are also reported.

Introduction

Probing the nature of bonds formed between actinide metals and other elements is important in expanding our understanding of the electronic structure and chemical bonding of the *f*-block elements, and in turn driving its evolution.[1-6] In the case of metal-metal bonds, those involving actinides are fundamentally different from their transition metal and lanthanide counterparts as a result of *f* orbital participation in bonding, coordinative diversity, and access to a wide range of oxidation states. Understanding these fundamental properties is of importance in nuclear fuel reprocessing, where small differences in covalency between the 4 and 5*f* elements may provide opportunities to improve separations.[7-10] Additionally, novel applications utilizing the actinides have recently emerged, including hydrocarbon functionalization, small molecule activation and group atom transfer reactions facilitated by uranium catalysts.[11]

The first actinide-transition metal bond, between Th and Ru, was reported by Marks and co-workers nearly thirty years ago.[12] In spite of this, *f*-element metal-metal bonds are still rare in comparison to the multitude of examples for the *s*, *p* and *d* block.[13-15] This is due in part to the fact that while there are a broad range of synthetic routes to metal-metal bonds involving transition metals in particular,[15] the synthesis of actinide analogues has been limited to salt metathesis and elimination reactions. Accordingly, only 17 structurally characterized examples have been reported,[16] establishing uranium bound to iron, ruthenium, rhenium and cobalt, in addition to the first example involving thorium.[17-23] Expanding the limited number of synthetic avenues to actinide metal-metal bonds provides an exciting opportunity to develop this field, with the potential to offer new insight into electronic structure and yield alternative modes of bimetallic cooperativity for novel catalytic applications.

The modular nitrogen/phosphorous scaffold, N[*o*-(NHCH$_2$P^{i}Pr$_2$)C$_6$H$_4$]$_3$ (N$_4$P$_3$), has recently been shown to facilitate metal-metal bonding via stabilization through the secondary phosphine coordination sphere, and has thus far been used to couple alumi-

Scheme 1. Synthesis of Thorium and Uranium Complexes 2-7[a]

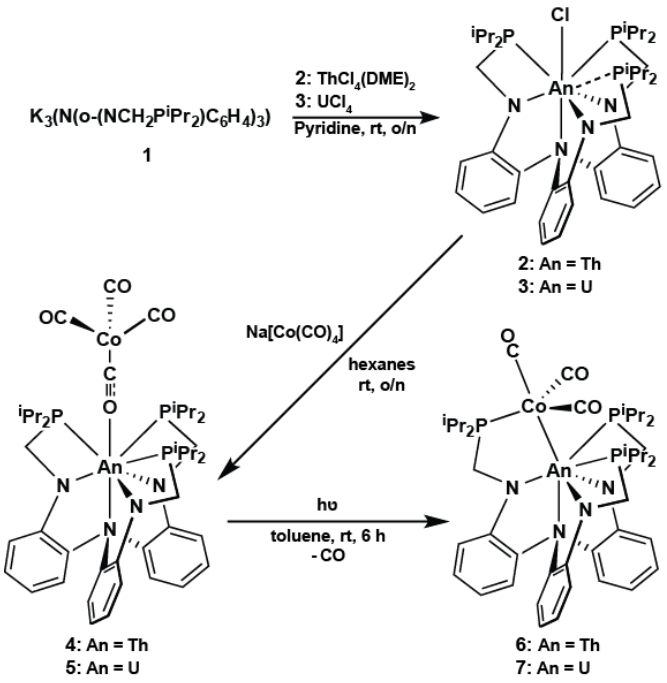

[a]Differences in phosphine binding in complexes 2 and 3 are indicated by a dotted line.

num and chromium with a series of first row transition metals.[24-26] Here, we show how this hard/soft donor system can be employed to provide a platform for bonding between (hard) actinides and (soft) late transition metals. Two important features of this approach are i) the intermediacy of an isocarbonyl $[Co(CO)_4]^-$ species that loses CO upon photolysis, and ii) the trapping of the resulting coordinatively unsaturated Co center by a pendent phosphine to yield the metal-metal bonded products. A series of uranium complexes, as well as their diamagnetic thorium analogues, has been synthesized. To the best of our knowledge, this method represents a new route to actinide-transition metal bonds, and results in a rare example of a U-Co bond as well as the first definitively characterized Th-Co bond.

Results and Discussion

Synthesis and Structural Properties. The potassium salt of the pro-ligand, K_3{N[*o*-$(NCH_2P^iPr_2)C_6H_4]_3$} (**1**), was prepared by reaction of the triamine with $K[N(TMS)_2]$ in toluene, affording the desired product in quantitative yield. Attempts to use the known lithium analogue were less successful, presumably due to salt incorporation - a common problem in metathesis chemistry with actinide metals. A uranium starting platform as well as the diamagnetic thorium analogue were targeted to allow for a wider range of characterization methods. Subsequently, the complexes {N[*o*-$(NCH_2P^iPr_2)C_6H_4]_3$}ThCl (**2**) and {N[*o*-$(NCH_2P^iPr_2)C_6H_4]_3$}UCl (**3**) were synthesized via combination of **1** with $ThCl_4(DME)_2$[27] and UCl_4[28] respectively in pyridine (Scheme 1). Both reactions were stirred at room temperature overnight, resulting in a pale yellow solution for the thorium complex **2**, and a dark red solution for uranium complex **3**. Evaporation of the solvent under vacuum, followed by crystallization from a mixture of diethyl ether (Et_2O) and hexanes at -40 °C, afforded colorless needles of **2** (65% yield) and orange needles of **3** (68% yield).

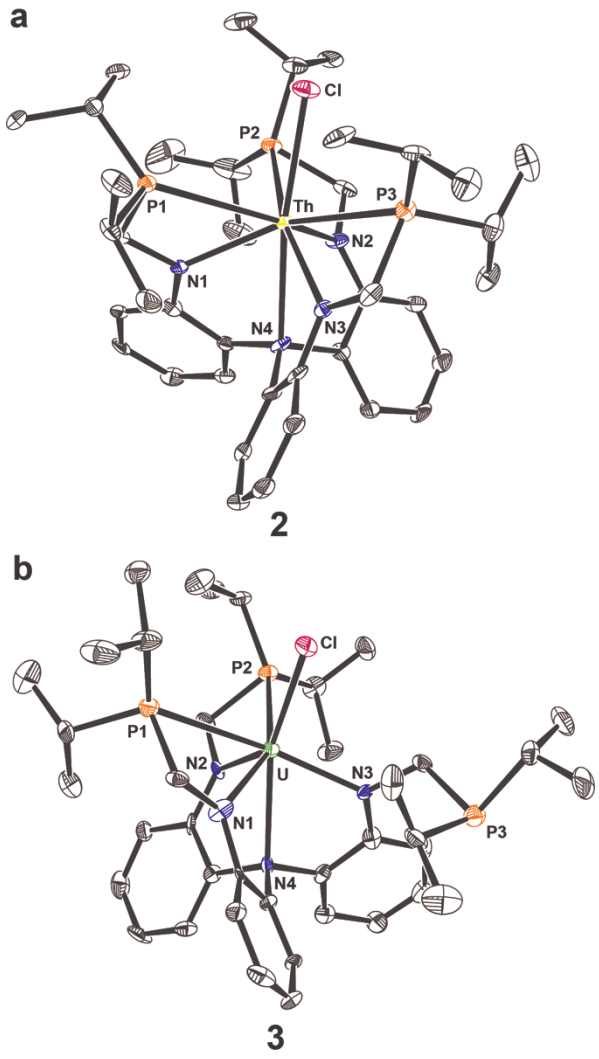

Figure 1. (a) Molecular structure of thorium complex **2** (b) Molecular structure of uranium complex **3**. Thermal ellipsoids are set to a 50% probability level and hydrogen atoms have been omitted for clarity.

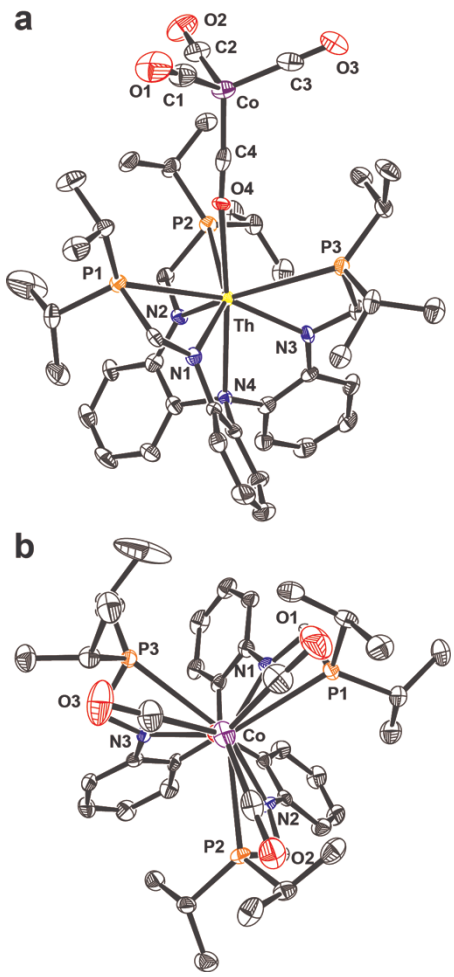

Figure 2. (a) Molecular structure of thorium complex 4 (b) Alternate view of 4 along the Co(μ-CO)Th axis, illustrating the staggered propeller conformation. Thermal ellipsoids are set to a 50% probability level and hydrogen atoms have been omitted for clarity.

The molecular structure of complex **2**, as determined by X-ray diffraction, reveals the coordination about the metal center to be eight coordinate (Figure 1a). Unlike the equivalent transition metal and main group complexes (and consistent with the much larger coordination sphere of the actinides) the phosphine arms interact with the actinide centers to varying degrees, in addition to the four nitrogen donors of the ligand. All three phosphines bind to the thorium center in **2**, but only two of the phosphine arms are coordinated in **3** (Figure 1b). This is consistent with the difference in ionic radii (1.00 Å vs. 1.05 Å for U(IV) and Th(IV) respectively).[29] Despite the small disparity, this variation is often enough to allow for a higher coordination number in the latter.[1] Complexes **2** and **3** represent a limited number of actinide complexes that employ ligands containing both a hard and soft donors. Utilizing similar ligand frameworks, highly reactive intermediates have been stabilized for further functionalization with transition metals and lanthanides, and **2** and **3** could provide a unique opportunity to establish orthogonal reactivity patterns using actinides.[30,31]

As an initial foray into exploring the capability of this platform to facilitate actinide metal-metal bonding, secondary metals known to bind favorably to the phosphine donors were targeted. Treatment of **2** or **3** with $Na[Co(CO)_4]$ in hexanes at room temperature overnight (Scheme 1) resulted in precipitation of the desired products from solution; crystallization from a mixture of toluene and hexanes at -40 °C yielded colorless blocks of **4** (77% yield) and dark orange blocks of **5** (76% yield). While there is well established literature precedent for carbonyl substitution by phosphines,[32,33] the oxophilicity of the actinide centers, coupled with the inherent stability of the $[Co(CO)_4]^-$ fragment, gave rise to less conventional isocarbonyl compounds **4** and **5**, as revealed by an X-ray diffraction study (Figures 2 and S1). Although there are many heterobimetallic transition metal isocarbonyls,[32,33] there are only five structurally characterized uranium isocarbonyls,[22,34,35] and we are unaware of any reports for thorium. Uniquely, **4** and **5** provide heterobimetallic systems suited to photolytic substitution via the carbonyls, while also possessing a secondary coordination sphere capable of stabilizing any resulting intermediates.

,The actinide centers for **4** and **5** are eight coordinate. All four nitrogens and the three phosphorus donors bind to the metal centers. Each complex displays a staggered conformation in relation to the $Co(CO)_3$, N_3An and P_3An units respectively (Figure 2b). The helical twist along the An-(μCO)-Co axis

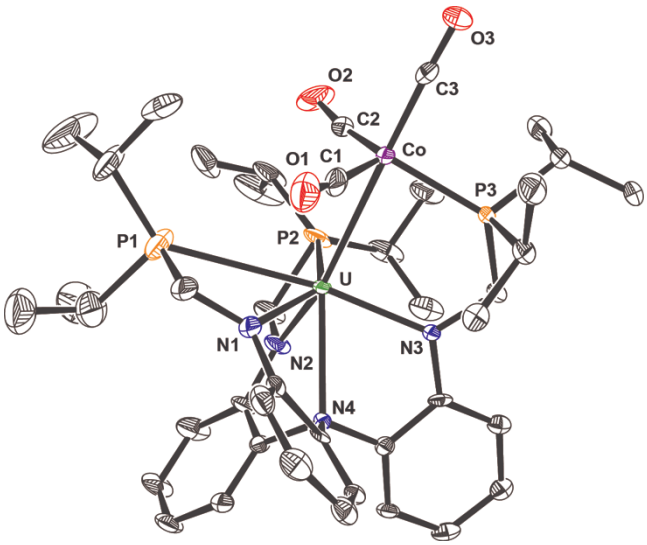

Figure 3. Molecular structure of uranium complex 7. Thermal ellipsoids are set to a 50% probability level and hydrogen atoms have been omitted for clarity.

results in torsion angles ranging from 23.43° to

33.44°, presumably to help minimize steric repulsions upon formation of the heterobimetallics.[36] The bond lengths and angles observed for **4** and **5** (Table S1) compare well with related uranium isocarbonyls, as well as a Yb compound having an analogous isocarbonyl bridged cobalt unit.[37]

Actinide-transition metal bonds were targeted via UV irradiation of compounds **4** and **5** as shown in Scheme 1. Evaporation of the solvent under vacuum, followed by crystallization from a mixture of Et_2O and hexanes at -40 °C, afforded colorless needles of **6** (61% yield) and red needles of **7** (58% yield). Unlike the bulk of literature concerning photolysis of transition metal carbonyl compounds, which describes either the irradiation of an existing metal-metal bond to promote dissociation, or the facilitation of ligand exchange,[32,33,38] irradiation of compounds **4** and **5** results in the formation of an actinide-metal bond (Figures 3 and S2). Formation of metal-metal bonds by this route is unusual for transition metals and, to our knowledge, has never been seen for actinides.[39-41] Subjecting the isolated compounds **4** and **5** to subsequent irradiation under the same conditions does not result in further carbonyl ligand substitution. Additionally, **6** and **7** do not react with CO under either thermal or photochemical conditions to reform **4** and **5**.

These compounds represent a unique system for comparing the variation in An-M bonding involving two different actinides with identical coordination spheres. The geometry about the metal centers is approximately trigonal bipyramidal, with τ values of 0.88 and 0.85 for the thorium and uranium complexes respectively.[42] The actinide-cobalt bond length is 3.0771(5) Å for **6** and 3.0319(7) Å for **7**. The sum of the covalent radii for thorium and cobalt and uranium and cobalt are 2.86 Å and 2.81 Å, respectively.[43] While longer than expected, the U-Co distance is within the range of limited examples present in the literature (2.9450(9) Å and 3.0812(7)-2.874(3));[23,44] there is no data to compare with in the case of Th-Co. The difference in bond lengths between **6** and **7** is consistent with the disparity in radii (either ionic or covalent) between thorium and uranium.

The actinide-cobalt bond is bent significantly with regard to the N4-An-Co angle (139° and 138° for **6** and **7**, respectively) as compared to the isocarbonyl precursors.. Interestingly, one of the cis carbonyls in each complex is tilted slightly towards the actinide center. The interaction, which does not appear to be a crystal packing effect, is more pronounced in the thorium example as indicated by both the Co-C2 (1.742(4) Å and 1.750(7) Å) and An-C2 (3.094(4) Å and 3.198(1) Å) distances in **6** and **7**, respectively, perhaps reflecting simply the difference in radii. Similar behavior has been observed for related carbonyl complexes with early transition metals.[36,45]

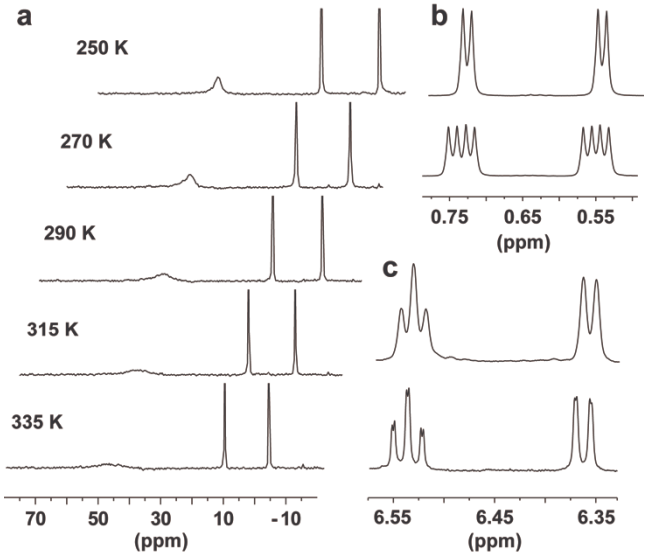

Figure 4. (a) Variable temperature ^{31}P NMR spectra of complex 6. (b) $^{1}H\{^{31}P\}$ (top) and ^{1}H NMR (bottom) spectra of two methyl groups of complex 4. (c) $^{1}H\{^{31}P\}$ (top) and ^{1}H NMR (bottom) spectra of two aromatic protons of complex 2. Both b and c illustrate the unique effect of phosphorous coupling observed

NMR Spectroscopy. The thorium complex **2** shows a ^{1}H NMR spectrum indicative of three-fold symmetry in solution (assignments were confirmed by phosphorous decoupled and proton-proton COSY NMR). However, unlike the analogous Al and Cr compounds of the N_4P_3 ligand, the methylene protons are diasterotopic, appearing as two doublets at 3.89 (J = 12 Hz) and 3.23 (J = 12 Hz) ppm. Additionally, all proton peaks show coupling to phosphorous, a feature that appears unique to the actinide compounds (Figure 4c). The ^{31}P NMR further confirms the three-fold symmetry, with a single resonance at 4.83 ppm. While the ^{1}H NMR spectrum for **3** is broad, paramagnetically shifted, and lacks any coherent splitting, the number of signals is in agreement with the symmetric thorium analogue. A phosphorous signal could not be detected, as is common in the presence of an f^2 uranium center (*see below*).

Table 1: Selected FTIR Data for Complexes 4-7

Compound	$\upsilon_{CO}(cm^{-1})$
Free CO	2143
$Na[Co(CO)_4]$	2024, 1878
4	2016, 1923, 1732
5	2013, 1922, 1748
6	1978, 1905, 1858
7	1977, 1907, 1864

Much like the starting chloride complex **2**, the solution state behavior of the thorium isocarbonyl **4** is indicative of three-fold symmetry, with the ^{1}H NMR resonances resembling those seen for **2**. The methylene protons remain diasterotopic at 3.55 (J = 12 Hz) and 3.05 (J = 12 Hz), again likely as a result of the phosphine coordination to the thorium center. There is a single ^{31}P NMR peak that is shifted to 6.41 ppm, indicating a small deshielding effect likely due to a slightly stronger interaction of the actinide center with the carbonyl.

The solution state behavior of the metal-metal bonded species **6** proves more complicated than either precursor, but upon careful inspection reflects the coordination seen in the solid state. The three-fold symmetry observed in thorium compounds **2** and **4** is absent for **6**. Instead, NMR spectroscopy indicates a loss of symmetry resulting from the coordination of a phosphine arm to the cobalt center upon loss of CO. Where there had previously been only one resonance per proton group in compounds **2** and **4**, three signals are observed in **6**. Accordingly, there are three signals in the ^{31}P NMR at 44.59, 9.43 and -6.59 ppm. The downfield resonance is broad, but in good agreement with phosphorous shifts reported for similar cobalt compounds.[36,46] Variable temperature experiments reveal a further broadening of the signal at higher temperatures and a sharpening at low temperatures (Figure 4a). Given the shift, and the dissimilarity from the other two signals, it seems likely that the broad signal corresponds to a cobalt-bound phosphine. The fluxional behavior could be due to an exchange of the ligand between the cobalt and the thorium, or the result of a Berry pseudorotation involving the carbonyls. Inequivalence of the remaining phosphorous atoms reflects the two different chemical environments observed in the solid-state structure.

Infrared Spectroscopy. In addition to providing a facile platform for exploring photolytic chemistry, the carbonyls of complexes **4**-**7** also supply a useful handle for examining the electronic structure of the series. Solid-state IR spectra of compounds **4** and **5** show two sharp CO stretches (Table 1) consistent with the approximate C_{3V} symmetry of the cobalt fragment seen in the crystal structures. Additionally, there is a broad stretch for the bridging carbonyls of **4** and **5** at 1732 cm^{-1} and 1748 cm^{-1} respectively. The dramatic weakening of this stretch is consistent with the electronic redistribution required to form the bridge, and is similar to the few examples reported for actinides mentioned earlier. The terminal CO stretches observed for **4** and **5** are significantly lower in energy than those seen in the cobalt starting material, indicating a significant redistribution of negative charge throughout the $[Co(CO)_4]^-$ unit via cobalt-carbonyl backbonding. This is also reflected in the expanding and contracting respectively of the $C123_{ave}$-$O123_{ave}$ and Co-$C123_{ave}$ distances, as well as the C4-O4 and Co-O4 values of the isocarbonyl (Table S1).

Electronic redistribution is also evident in the solid-state IR spectra of compounds **6** and **7**, which show three sharp CO stretches consistent with the geometry and CO coordination number to the cobalt unit seen in the crystal structure. The CO stretch of the carbonyl trans to the metal-metal bond provides a probe of the interaction strength and is indeed the only stretch with a significant disparity between the two complexes.[36] The stretch is weaker in the thorium example, which could be attributed to a stronger metal-metal interaction in the uranium case, causing in turn a weaker backbonding from the cobalt to the carbonyl. Additionally, the stretches for **6** and **7** are weaker than for those of their isocarbonyl counterparts and consistent with a polarization of charge from the cobalt to the actinide center and a corresponding decrease in Co-CO backbonding.

Magnetic Susceptibility. As an additional means of evaluating the electronic structure of the uranium series, variable temperature magnetic susceptibilies, χ, of complexes **3**, **5** and **7** were measured in the solid state (Figure 5). The effective magnetic moments of **3**, **5** and **7** at 300 K are 2.6, 2.7, and 3.2 Bohr magnetons (μ_B), respectively. This value is lower than the free ion magnetic moments of both U(III) and U(IV), which is 3.6 μ_B in both cases (ref: Castro-Rodriguez, I.; Olsen, K.; Gantzel, P.; Meyer, K. *J. Am. Chem. Soc.* **2003**, *125*, 4565-4571). Both crystal field splitting and covalency can affect the magnetic moment, so the room temperature moment alone cannot allow one to determine the uranium oxidation state. The observed values are similar to those reported for both U(III) and U(IV) amide complexes.(refs: King, D.M.; Lewis, W.; Liddle, S.T. Inorganica Chimica Acta (2012), 380, 167-173; Lewis, A.J.; Williams, U.J.; Kikkawa, J.M.; Carroll,

P.J.; Schelter, E.J. Chemistry (2012), 51(1), 37-39; Patel, D.; Lewis, W.; Blake, A.J.; Liddle, S.T. Dalton Transactions (2010), 39(29), 6638-6647; Castro-Rodriguez, I.; Olsen, K.; Gantzel, P.; Meyer, K. Journal of the American Chemical Society (2003), 125(15), 4565-4571; Reynolds, J.G.; Edelstein, N. M. Inorganic Chemistry (1977), 16(11), 2822-5; Andersen, R.A. Inorganic Chemistry (1979), 18(6), 1507-9)

For **3**, **5** and **7**, μ_{eff} decreases towards zero as the temperature is lowered, which is consistent with U(IV), which has an f^2, $^3H_4$ configuration with a singlet ground state.[1] The temperature independent ground state is indicated in the χ vs. T plot by a change in slope where first excited state becomes thermally populated (indicated by arrows in Figure 5). In **5**, the ground state is least magnetic and is the only appreciably populated state up to ~100 K. In **3**, the ground state has a greater magnetic susceptibility and persists to a somewhat lower temperature, ~70 K. In **7**, the ground state has the greatest magnetic susceptibility and persists to ~60 K..

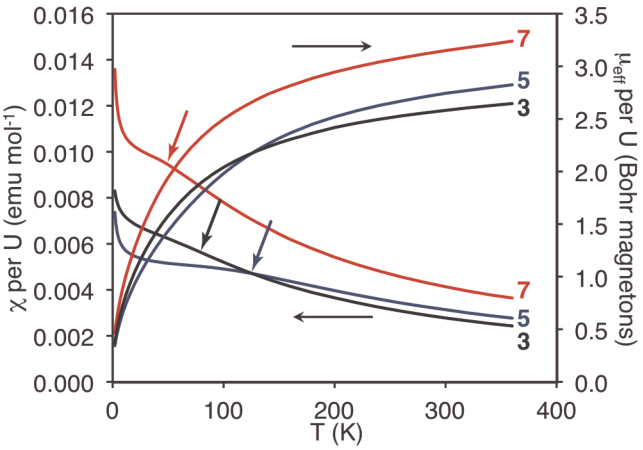

Figure 5. Variable-temperature magnetic susceptibility of complexes 3, 5 and 7. The change in slope due to thermal population of the first excited state is marked by an arrow.

Both the magnetic susceptibility of the singlet state and the temperature over which this state is exclusively occupied are functions of the strength of the crystal field. Stronger ligands lead to larger splitting between the ground state and higher lying states, which decreases the susceptibility of the ground state and the increases the temperature over which it is solely occupied. The splitting of the $^3H_4$ state is greatest in **5** and smallest in **7**. This mirrors the bond distances observed between the uranium center and the apical ligand with the shortest (U-OC) in **5** and longest (U-Co) in **7**. In agreement with the crystallographic and NMR data presented previously, this suggests that the isocarbonyl displays the strongest interaction with the U(IV) center and Co has the weakest, which underscores the necessity to employ photolytic excitation to enable the formation of the An-Co bond via ligand exchange.

UV-Vis/NIR Spectroscopy. Finally, the electronic structure of the uranium series was investigated using UV-Vis/NIR spectroscopy (Figure 6). Complexes **3**, **5** and **7** display a broad shoulder at ~300 nm, followed by a peak at ~430 nm, showing shifts consistent with the gradual orange-to-red color change observed across the series. Both peaks are similar to those reported for the analogous Al and Cr compounds of the ligand and are consistent with π-π^* transitions in the ligand backbone and M-L charge transfer, respectively. Additionally, there are several sharp peaks not seen in the main group or transition metal compounds at ~675 nm (ε = ~1.25 x 10^2 M^{-1} cm^{-1}), consistent with *f*-based transitions. In contrast to the UV-vis region, the broad peaks in the NIR spectra are distinct between compounds. The uranium chloride complex **3** displays a single peak at 1064 nm (ε = 0.97 x 10^2 M^{-1} cm^{-1}), similar to that reported for the aluminum-cobalt complex. However, the isocarbonyl complex **5** displays two peaks at 1024 nm (ε = 1.12 x 10^2 M^{-1} cm^{-1}) and 1056 nm (ε = 1.17 x 10^2 M^{-1} cm^{-1}), and the U-Co bound complex **7** displays a more intense single peak at 1058 nm (ε = 2.16 x 10^2 M^{-1} cm^{-1}). Metal-based transitions were observed in the NIR region for the corresponding main group and transition metal examples of this ligand. Likewise, the two peaks observed for isocarbonyl **5** may arise due to independent cobalt and uranium based transitions. Subsequently, and consistent with the polarization of charge between the metal centers in **7**, a single transition of increased intensity is seen upon formation of the U-Co bond.

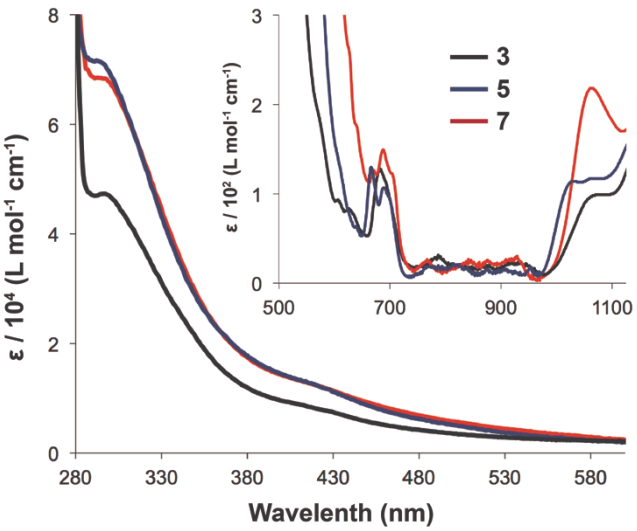

Figure 6. UV-visible absorption spectra of complexes **3**, **5** and **7** in toluene. Inlay: NIR absorption spec-

Conclusions

This work shows that actinide-transition metal bonds can be generated via photolysis of isocarbonyl complexes. A key design feature of this work is the ready availability of a pendent phosphine ligand, unique to the N_4P_3 ligand scaffold. The secondary coordination sphere appears to be crucial to the formation of actinide-metal bonds upon photolysis since without it, the resulting coordinatively unsaturated $Co(CO)_3$ complex would likely decompose. In this way, we have generated two new An-Co complexes, including one featuring a previously unknown Th-Co bond. We believe this approach represents a new way to create actinide-metal bonds and may provide a rich platform for expanding the study of actinide metal-metal bonding and associated reactivity.

Experimental details

General procedures. Unless otherwise noted, all reactions were performed using standard Schlenk line techniques or in an MBraun N_2-atmosphere glovebox (< 1 ppm O_2/H_2O). All glassware and Celite® were stored in an oven at ca. 150 °C. Dimethoxyethane (DME), diethyl ether (Et_2O), toluene, hexanes, pentane and pyridine were dried and degassed using a Phoenix Solvent Drying System commercially available from JC Meyer Solvent Systems. Hexamethyldisiloxane (HMDSO) was vacuum-transferred from CaH_2 and degassed with three freeze-pump-thaw cycles. Deuterated solvents were vacuum-transferred from either sodium/benzophenone (C_6D_6 and toluene-d_8) or CaH_2 (pyridine-d_5) and degassed with three freeze-pump-thaw cycles. All NMR spectra were recorded at the specified temperature on Bruker AVQ-400, DRX 500 or AV-600 spectrometers. Temperature calibration was performed using changes in chemical shift separation of ethylene glycol at high temperature, and methanol at low temperature. ^{1}H chemical shifts (δ) were calibrated using residual solvent peaks. ^{31}P chemical shifts (δ) were referenced to an external standard (Ph_3PO at 23 ppm). UV-visible and near infrared (NIR) spectra were collected in toluene and determined with a UV-3101PC scanning spectrophotometer, using a Schlenk-adapted 1 mm quartz cell. Infrared (IR) spectra were recorded with a Thermo Scientific Nicolet iS10 FTIR spectrophotometer either as powder, or as Nujol mulls between KBr plates. Melting points were determined on an Optmelt SRS using sealed capillaries prepared under nitrogen and are uncorrected. Photolysis was conducted using a Rayonet reactor (Model RPR-100) centered at 253 nm with approximately 1.65 x 10^{16} photons/sec/cm^3. The ligand N[*o*-$(NCH_2P^iPr_2)C_6H_4]_3$, $ThCl_4(DME)_2$,[27] UCl_4[28] and $Na[Co(CO)_4]$[47] were prepared according to literature procedures.

K_3{N[*o*-$(NCH_2P^iPr_2)C_6H_4]_3$} **(1).** A solution of the ligand N[*o*-$(NCH_2P^iPr_2)C_6H_4]_3$ (2.0 g, 2.9 mmol) in toluene (40 mL) was added to a suspension of $K[N(TMS)_2]$ (1.9 g, 9.7 mmol) in toluene (40 mL) to produce a yellow solution. The reaction mixture was stirred for 1 d, resulting in the precipitation of a yellow solid. The reaction mixture was filtered and washed with hexanes (2 x 5 mL) to afford the desired product as a pale yellow solid (2.33 g, 99% yield). ^{1}H NMR (400 MHz, pyridine-d_5, 293 K): δ 7.24 (d, 1H, Ar-*H*, *J* = 8.0 Hz), 7.04 (t, 1H, Ar-*H*, *J* = 8.0 Hz), 6.47 (d, 1H, Ar-*H*, *J* = 8.0 Hz), 5.93 (t, 1H, Ar-*H*, *J* = 8.0 Hz), 3.42 (ABq, 2H, CH_2, $\Delta\delta_{AB}$ = 0.13, J_{AB} = 16 Hz), 1.77 (m, 2H, C*H*), 1.11 (m, 12H, CH_3). ^{31}P NMR (400 MHz, pyridine-d_5): δ 2.00. Mp: dec. > 164 ºC.

{N[*o*-$(NCH_2P^iPr_2)C_6H_4]_3$}ThCl (2). A solution of **1** (1.1 g, 1.4 mmol) in pyridine (25 mL) was added to a suspension of $ThCl_4(DME)_2$ (766 mg, 1.4 mmol) in pyridine (25 mL) to produce an off white suspension. The reaction mixture was stirred for 12 h, resulting in a pale yellow solution. The solvent was removed in vacuo to yield a pale orange solid. The solid was extracted with ether (3 x 10 mL), filtered, and concentrated until saturation. Hexanes were added dropwise until cloudy and the solution was then chilled for 2 d at -40 ºC to afford the product as colorless needles (843 mg, 65% yield). Single crystals suitable for X-ray diffraction were obtained from a concentrated solution of **2** in pentane stored at -40 °C for 12 hr. ^{1}H NMR (600 MHz, C_6D_6, 293 K): δ 7.18 (t, partially obscured by solvent, 1H, Ar-*H*, *J* = 6.0 Hz), 7.07 (d, 1H, Ar-*H*, *J* = 12 Hz), 6.53 (t, 1H, Ar-*H*, *J* = 9.0 Hz), 6.36 (d, 1H, Ar-*H*, *J* = 6.0 Hz), 3.89 (d, 1H, CH_2, *J* = 12 Hz), 3.23 (d, 1H, CH_2, *J* = 12 Hz), 2.06 (sept, 1H, C*H*, *J* = 6.0 Hz), 1.57 (sept, 1H, C*H*, *J* = 6.0 Hz), 1.27 (d, 3H, CH_3, *J* = 6.0 Hz), 1.24 (d, 3H, CH_3, *J* = 6.0 Hz), 0.84 (d, 3H, CH_3, *J* = 6.0 Hz), 0.66 (d, 3H, CH_3, *J* = 6.0 Hz). ^{31}P NMR (600 MHz, C_6D_6, 293 K): δ 4.83. Anal. Calcd (%) for $C_{39}H_{60}ClN_4P_3Th$: C, 49.55; H, 6.40; N, 5.93. Found: C, 49.17; H, 6.69; N, 5.82. Mp: dec. > 138 ºC.

{N[*o*-$(NCH_2P^iPr_2)C_6H_4]_3$}UCl (3). A solution of **1** (1.0 g, 1.3 mmol) in pyridine (25 mL) was added to a suspension of UCl_4 (480 mg, 1.3 mmol) in pyridine (25 mL) to produce a red suspension. The reaction mixture was stirred for 12 h, resulting in a dark red solution. The solvent was removed in vacuo to yield a dark orange solid. The solid was extracted with Et_2O (3 x 10 mL), filtered, and concentrated until saturation. Hexanes were added dropwise until cloudy and the solution was then chilled for 1 d at -40 ºC to

afford the product as orange needles (807 mg, 68% yield). Single crystals suitable for X-ray diffraction were obtained from a concentrated solution of **3** in pentane stored at -40 °C for 12 h. ^{1}H NMR (400 MHz, C_6D_6, 293 K): δ 37.92 (s, br), 22.49 (s, br), 11.58 (s, br), 10.91 (s, br), 9.41 (s, br), 8.67 (m, br), 7.03 (s, br), 5.65 (s, br), 1.22 (m, br), -2.70 (s, br), -4.82 (s, br), -6.64 (s, br). UV-Vis/NIR [nm, ε (M^{-1} cm^{-1})]: 298, 47,100; 431, 7,320; 680, 129; 1064, 97. Anal. Calcd (%) for $C_{39}H_{60}ClN_4P_3U$: C, 49.23; H, 6.36; N, 5.89. Found: C, 49.34; H, 6.45; N, 6.01. Mp: dec. > 145 ºC. μ_{eff} = 2.6 μ_B at 300 K.

{N[*o*-(NCH$_2$P^{i}Pr$_2$)C$_6$H$_4$]$_3$}Th(μ-OC)Co(CO)$_3$ (4). A solution of **2** (100 mg, 0.10 mmol) in toluene (2 mL) was added to a suspension of Na[Co(CO)$_4$] (21 mg, 0.10 mmol) in toluene (2 mL) to produce a pale yellow suspension. The reaction mixture was stirred for 12 h, resulting in a yellow solution and a fine white precipitate. The solvent was removed in vacuo to yield an off-white solid. The solid was extracted with toluene (3 x 2 mL), filtered, and concentrated until saturation. Hexanes were added dropwise until cloudy and the solution was then chilled for 1 d at -40 ºC to afford the product as colorless blocks (88 mg, 77% yield). Single crystals suitable for X-ray diffraction were obtained from a concentrated solution of **4** in toluene stored at -40 °C for 12 h. ^{1}H NMR (600 MHz, C_6D_6, 293 K): δ 7.08 (t, 1H, Ar-*H*, *J* = 9.0 Hz), 7.02 (d, 1H, Ar-*H*, *J* = 6.0 Hz), 6.51 (t, 1H, Ar-*H*, *J* = 9.0 Hz), 6.11 (d, 1H, Ar-*H*, *J* = 6.0 Hz), 2.15 (sept, 1H, C*H*, *J* = 6.0 Hz), 1.46 (sept, 1H, C*H*, *J* = 6.0 Hz), 1.31 (d, 3H, C*H*$_3$, *J* = 6.0 Hz), 1.28 (d, 3H, C*H*$_3$, *J* = 6.0 Hz), 0.77 (d, 3H, C*H*$_3$, *J* = 6.0 Hz), 0.59 (d, 3H, C*H*$_3$, *J* = 6.0 Hz). ^{31}P NMR (600 MHz, C_6D_6, 293 K): δ 6.41. IR (cm^{-1}): 2016 (m, CO), 1923 (s, CO), 1733 (s, CO), 1586 (m), 1310 (m), 1290 (m), 1234 (w), 1157 (w), 1116 (w), 1040 (w), 745 (m), 722 (m), 563 (m), 512 (m). Anal. Calcd (%) for $C_{43}H_{60}CoN_4O_4P_3Th$: C, 47.78; H, 5.60; N, 5.18. Found: C, 35.29; H, 3.63; N, 5.09. The isocarbonyl compounds are subject to very rapid thermal and photolytic decomposition unless kept frozen and in a dark environment. Therefore it is unsurprising that the found percentages for elemental analysis are not in good agreement. Mp: dec. > 136 ºC.

{N[*o*-(NCH$_2$P^{i}Pr$_2$)C$_6$H$_4$]$_3$}U(μ-OC)Co(CO)$_3$ (5). A solution of **3** (330 mg, 0.34 mmol) in toluene (2 mL) was added to a suspension of Na[Co(CO)$_4$] (66 mg, 0.34 mmol) in toluene (2 mL) to produce an orange suspension. The reaction mixture was stirred for 12 h, resulting in a red solution and a fine white precipitate. The solvent was removed in vacuo to yield an orange solid. The solid was extracted with toluene (3 x 2 mL), filtered, and concentrated until saturation. Hexanes were added dropwise until cloudy and the solution was then chilled for 1 d at -40 ºC to afford the product as orange blocks (281 mg, 76% yield). Single crystals suitable for X-ray diffraction were obtained from a concentrated solution of **5** in toluene stored at -40 °C for 12 h. ^{1}H NMR (400 MHz, C_6D_6, 293 K): δ 52.86 (s, br), 23.92 (s, br), 16.58 (s, br), 12.66 (m, br), 10.29 (s, br), 8.39 (m, br), 8.31 (s, br), 3.44 (m, br), 0.29 (s, br), -2.04 (m, br), -3.13 (s, br), -12.93 (s, br). IR (cm^{-1}): 2013 (m, CO), 1922 (s, CO), 1748 (s, CO), 1586 (m), 1310 (m), 1290 (m), 1234 (w), 1157 (w), 1116 (w), 1049 (w), 747 (m), 722 (m), 560 (m), 517 (m). UV-Vis/NIR [nm, ε (M^{-1} cm^{-1})]: 296, 71,100; 429, 13,100; 668, 127; 693, 104; 1024, 112; 1056, 117. Anal. Calcd (%) for $C_{43}H_{60}CoN_4O_4P_3U$: C, 47.52; H, 5.56; N, 5.16. Found: C, 41.34; H, 3.86; N, 4.83. Mp: dec. > 149 ºC. μ_{eff} = 2.7 μ_B at 300 K.

{N[*o*-(NCH$_2$P^{i}Pr$_2$)C$_6$H$_4$]$_3$}ThCo(CO)$_3$ (6). A solution of **4** (130 mg, 0.12 mmol) in toluene (2 mL) was irradiated with ultraviolet light (centered at 254 nm) for 12 h, resulting in a color change from pale yellow to yellow. The solvent was removed in vacuo to yield a pale yellow solid. The solid was extracted with Et_2O (3 x 2 mL), filtered, and concentrated until saturation. The solution was then chilled for 1 d at -40 ºC to afford the product as colorless blocks (79 mg, 61% yield). Single crystals suitable for X-ray diffraction were obtained by vapor diffusion at -40 °C of hexane into a concentrated solution of **6** in toluene. ^{1}H NMR (600 MHz, C_6D_6, 293 K): δ 7.23 (t, 1H, Ar-*H*, *J* = 6.0 Hz), 7.19 (t, 1H, Ar-*H*, *J* = 6.0 Hz), 7.12 (m, 2H, Ar-*H*), 7.06 (d, 1H, Ar-*H*, *J* = 6.0 Hz), 6.95 (d, 1H, Ar-*H*, *J* = 6.0 Hz), 6.61 (m, 2H, Ar-*H*), 6.52 (t, 1H, Ar-*H*, *J* = 6.0 Hz), 6.49 (t, 1H, Ar-*H*, *J* = 6.0 Hz), 6.42 (d, 1H, Ar-*H*, *J* = 6.0 Hz), 6.14 (d, 1H, Ar-*H*, *J* = 6.0 Hz), 4.38 (d, 1H, C*H*$_2$, *J* = 12 Hz), 3.97 (d, 1H, C*H*$_2$, *J* = 12 Hz), 3.62 (d, 1H, C*H*$_2$, *J* = 12 Hz), 3.36 (m, 2H, C*H*$_2$), 3.14 (d, 1H, C*H*$_2$, *J* = 12 Hz), 2.43 (sept, 1H, C*H*, *J* = 6.0 Hz), 2.00 (sept, 1H, C*H*, *J* = 6.0 Hz), 1.87 (m, 2H, CH), 1.77 (sept, 1H, C*H*, *J* = 6.0 Hz), 1.57 (sept, 1H, C*H*, *J* = 6.0 Hz), 1.43 (d, 3H, C*H*$_3$, *J* = 12 Hz), 1.39 (d, 3H, C*H*$_3$, *J* = 6.0 Hz), 1.27 (d, 3H, C*H*$_3$, *J* = 6.0 Hz), 1.11 (d, 3H, C*H*$_3$, *J* = 6.0 Hz), 0.94 (m, 9H, C*H*$_3$), 0.86 (d, 3H, C*H*$_3$, *J* = 6.0 Hz), 0.81 (d, 3H, C*H*$_3$, *J* = 12 Hz), 0.74 (d, 3H, C*H*$_3$, *J* = 6.0 Hz), 0.62 (m, 6H, C*H*$_3$). ^{31}P NMR (600 MHz, C6D6, 293 K): δ 44.59, 9.43, -6.59. IR (cm^{-1}): 1979 (s, CO), 1905 (s, CO), 1858 (s, CO), 1591 (m), 1310 (m), 1290 (m), 1254 (w), 1156 (w), 1117 (w), 1040 (w), 856 (w), 743 (m), 727 (m). Anal. Calcd (%) for $C_{42}H_{60}CoN_4O_3P_3Th$: C, 47.91; H, 5.74; N, 5.32. Found: C, 48.04; H, 5.86; N, 5.19. Mp: dec. > 160 ºC.

{N[*o*-(NCH$_2$P^{i}Pr$_2$)C$_6$H$_4$]$_3$}UCo(CO)$_3$ (7). A solution of **5** (150 mg, 0.14 mmol) in toluene (2 mL)

was irradiated with ultraviolet light (centered at 254 nm) for 12 h, resulting in a color change from orange to red. The solvent was removed in vacuo to yield a red solid. The solid was extracted with Et_2O (3 x 2 mL), filtered, and concentrated until saturation. The solution was then chilled for 1 d at -40 ºC to afford the product as red blocks (87 mg, 58% yield). Single crystals suitable for X-ray diffraction were obtained from a concentrated solution of **7** in HMDSO stored at -40 °C for 12 h. ^{1}H NMR (400 MHz, C_6D_6, 293 K): δ 88.56 (s, br), 75.00 (s, br), 51.45 (s, br), 38.96 (s, br), 28.70 (s, br), 27.11 (s, br) 20.06 (s, br), 17.34 (s, br) 17.05 (s, br), 16.45 (s, br), 16.05 (s, br), 14.41 (s, br), 11.84 (s, br), 11.72 (s, br), 11.29 (m, br), 11.10 (m, br), 9.17 (s, br), 8.32 (s, br), 7.91 (s, br), 7.52 (s, br), 6.42 (s, br), 3.39 (m, br), 2.68 (m, br), 2.17 (s, br), -1.84 (s, br), -2.05 (m, br), -9.41 (m, br), -10.95 (s, br), -11.57 (s, br), -11.79 (s, br), -15.67 (s, br), -19.01 (s, br), -24.40 (s, br), -26.25 (s, br). IR (cm^{-1}): 1977 (s, CO), 1908 (s, CO), 1864 (s, CO), 1590 (m), 1310 (m), 1288 (m), 1253 (w), 1155 (w), 1117 (w), 1048 (w), 846 (w), 742 (m), 722 (m). UV-Vis/NIR [nm, ε (M^{-1} cm^{-1})]: 299, 69,800; 433, 10,900; 669, 124; 689, 149; 1058, 216. Anal. Calcd (%) for $C_{42}H_{60}CoN_4O_3P_3U$: C, 47.64; H, 5.71; N, 5.29. Found: C, 47.52; H, 5.79; N, 5.16. Mp: dec. > 145 ºC. μ_{eff} = 3.0 μ_B at 300 K.

Crystallographic procedures. X-ray structural determinations were performed at CHEXRAY, University of California, Berkeley, on a Bruker APEX II Quazar diffractometer. The instrument is Kappa Geometry with DX, and is a 3-circle diffractometer that couples a CCD detector[48] with a sealed-tube source of monochromatized Mo Kα radiation. A crystal of appropriate size was coated in Paratone-N oil and mounted on a Kaptan® loop. The loop was transferred to the diffractometer, centered in the beam, and cooled by a nitrogen flow low-temperature apparatus that had been previously calibrated by a thermocouple placed at the same position as the crystal. Preliminary orientation matrices and cell constants were determined by collection of 60 10 s frames, followed by spot integration and least-squares refinement. The reported cell dimensions were calculated from all reflections with I > 10 σ. The data were corrected for Lorentz and polarization effects; no correction for crystal decay was applied. An empirical absorption correction based on comparison of redundant and equivalent reflections was applied using SADABS.[49] All software used for diffraction data processing and crystal-structure solution and refinement are contained in the APEX2 program suite (Bruker AXS, Madison, WI).[50] Thermal parameters for all non-hydrogen atoms were refined anisotropically. For all structures, R1 = Σ(|Fo| - |Fc|)/Σ(|Fo|); wR2 = [Σ{w(Fo2 - Fc2)2}/Σ{w(Fo2)2}]1/2, ORTEP diagrams were created using the ORTEP-3 software package and POV-ray.[51,52]

Magnetism procedures. Uranium complexes **3**, **5** and **7** (x mg) were sandwiched between two plugs of quartz wool (Hereaus, x mg) in a 4 mm OD quartz tube, which was flame sealed on both ends. Sample magnetization was recorded at 0.1 T, 0.5 T, and 1 T using a Quantum Designs MPMS SQUID magnetometer. Magnetization was corrected for the diamagnetism of the quartz wool using Pascal's constants (no correction for the diamagnetism of the quartz tube is needed as the quartz tube never leaves the SQUID coils). Molar susceptibility was corrected for the presence of a small amount of ferromagnetic impurity (M_{ferro}), the diamagnetism of the quart wool (χ_{QW}), ligands and uranium (χ_{dia}) using Pascal's constants, and calculated using the following equation:

$$\chi_{mol} = \frac{(\text{molecular weight})}{(\text{sample mass})}\left[\frac{(M_{meas} - M_{ferro})}{H} - \chi_{QW}\right] - \chi_{dia}$$

where χ_{mol} is the molar susceptibility, M_{meas} is the measured magnetization, M_{ferro} is the magnetization of the ferromagnetic impurity, which is temperature independent and assumed to be identical at all fields, χ_{QW} is the contribution to the susceptibility due to the quartz wool, χ_{dia} is the diamagnetic correction, and H is the applied field. For **3** and **5**, this equation was applied to the 0.5 T and 1 T data to determine, M_{ferro}, which was $1.6x10^{-5}$ emu and $2.92x10^{-5}$ emu, respectively. The 0.1 T data was fit to the other data using $M_{ferro,0.1T}$ = 0.63 M_{ferro} because the 0.1 T data is below the anisotropy field of the ferromagnetic impurity (see below); the value of 0.63 was determined by fitting the 0.1 T data to the 0.5 T and 1 T data. For **7**, the amount of ferromagnetic impurity was determined using the 0.1 T, 0.5 T and 1 T data and $M_{ferro,0.1T}$ = 0.63 M_{ferro}; M_{ferro} = $1.6x10^{-5}$ emu.

Two ferromagnetic impurities are commonly encountered in laboratory samples, steel or iron metal and magnetite or other ferrites from oxide coating on stainless steel lab equipment. Of these, magnetite is far more likely to be encountered. In general, the magnetization of ferromagnets is temperature independent below the Curie temperature, which is 860 K for magnetite, respectively, so magnetization of the impurity is temperature independent for this experiment. The magnetization of ferromagnets is also largely field-independent above the anisotropy field, which is approximately 0.2 T for magnetite, above which the magnetization is ~90 emu/g. (ref Morales, M.A.; Jain, T.K.; Labhasetwar, V; Leslie-Pelecky,

D.L. *J. Appl. Phys.* **2005**, *97*, 10Q905). Below the anisotropy field, the magnetization of a magnet is roughly linear with applied field. Based on the assumption that the impurity is magnetite or some other ferrite resulting from the abrasion of stainless steel lab equipment, the data were corrected for a temperature and field independent ferromagnetic impurity. M_{ferro} was allowed to vary to minimize least squares difference between χ_{mol} at different fields, which produced a saturation magnetization of $M_{ferro} \sim 2\times10^{-5}$ emu (actual values in SI), which corresponds to ~0.2 ug of magnetite. Data before and after correction for the presence of the ferromagnetic impurity are shown in Figures S3 through S8.

ASSOCIATED CONTENT

Supporting Information. The molecular structures of complexes **5** and **6**, as well as crystallographic data and refinement parameters for complexes **2-7** (CIF), and additional magnetic susceptibility data are available free of charge via the Internet at http://pubs.acs.org.

AUTHOR INFORMATION

Corresponding Author

arnold@berkeley.edu

ACKNOWLEDGMENT

ALW acknowledges the NSF for a GFRP fellowship and UC Berkeley for a Dissertation Year Fellowship. We are grateful to Nick Kornienko (NIR), Antonio DiPasquale (XRD) and Thomas Gianetti (NMR) for assistance with instrumentation, as well as Drs. Casey Brown and Stefan Minasian for helpful discussions. This work was supported by U.S. Department of Energy, Office of Basic Energy Sciences, Chemical Sciences, Biosciences, and Geosciences Division, and a portion was performed at Lawrence Berkeley National Laboratory under Contract No. DE-AC02-05CH11231

REFERENCES

(1) Morss, L. R., Edelstein, N., Fuger, J. *The Chemistry of the Actinide and Transactinide Elements*, 3rd ed.; Springer: Dordrecht, The Netherlands, 2006.

(2) Jones, M. B.; Gaunt, A. J. *Chem Rev* **2013**, *113*, 1137–1198.

(3) Liddle, S. T.; Mills, D. P. *Dalton T* **2009**, 5592.

(4) Ephritikhine, M. *Dalton T* **2006**, 2501.

(5) Minasian, S. G.; Krinsky, J. L.; Arnold, J. *Chem-Eur J* **2011**, *17*, 12234–12245.

(6) Edelmann, F. T. *Coordin Chem Rev* **2013**, *257*, 1122–1231.

(7) International Atomic Energy Agency *Spent Fuel Reprocessing Options*; International Atomic Energy Agency, **2009**.

(8) *Nuclear Energy Advisory Committee Report*, U.S. Department of Energy, **2008**.

(9) Kozimor, S. A.; Yang, P.; Batista, E. R.; Boland, K. S.; Burns, C. J.; Clark, D. L.; Conradson, S. D.; Martin, R. L.; Wilkerson, M. P.; Wolfsberg, L. E. *J Am Chem Soc* **2009**, *131*, 12125–12136.

(10) Arnold, P. L.; Turner, Z. R.; Kaltsoyannis, N.; Pelekanaki, P.; Bellabarba, R. M.; Tooze, R. P. *Chem-Eur J* **2010**, *16*, 9623–9629.

(11) Fox, A. R.; Bart, S. C.; Meyer, K.; Cummins, C. C. *Nature* **2008**, *455*, 341–349.

(12) Sternal, R. S.; Brock, C. P.; Marks, T. J. *J Am Chem Soc* **1985**, *107*, 8270–8272.

(13) Green, S. P.; Jones, C.; Stasch, A. *Science* **2007**, *318*, 1754–1757.

(14) Schnöckel, H. *Dalton T* **2008**, 4344.

(15) Cotton, F. A.; Murillo, C. A.; Walton, R. A. *Multiple Bonds Between Metal Atoms*, 3rd ed.; Springer Science: New York, NY, **2005**.

(16) Chang, C.; Loh, Z.; Shi, C.; Anson, F.; Nocera, D. *J Am Chem Soc* **2004**, *126*, 10013–10020.

(17) Bucaille, A.; Le Borgne, T.; Ephritikhine, M.; Daran, J. C. *Organometallics* **2000**, *19*, 4912–4914.

(18) Monreal, M. J.; Khan, S. I.; Kiplinger, J. L.; Diaconescu, P. L. *Chemical Communications* **2011**, *47*, 9119.

(19) Gardner, B. M.; Mcmaster, J.; Lewis, W.; Liddle, S. T. *Chemical Communications* **2009**, 2851.

(20) Patel, D.; King, D. M.; Gardner, B. M.; Mcmaster, J.; Lewis, W.; Blake, A. J.; Liddle, S. T. *Chemical Communications* **2010**, *47*, 295.

(21) Gardner, B. M.; Patel, D.; Cornish, A. D.; Mcmaster, J.; Lewis, W.; Blake, A. J.; Liddle, S. T. *Chem-Eur J* **2011**, *17*, 11266–11273.

(22) Patel, D.; Moro, F.; Mcmaster, J.; Lewis, W.; Blake, A. J.; Liddle, S. T. *Angew Chem Int Edit* **2011**, *50*, 10388–10392.

(23) Napoline, J. W.; Kraft, S. J.; Matson, E. M.; Fanwick, P. E.; Bart, S. C.; Thomas, C. M. *Inorg Chem* **2013**, 131010155347009.

(24) Rudd, P. A.; Liu, S.; Gagliardi, L.; Young, V. G.; Lu, C. C. *J Am Chem Soc* **2011**, *133*, 20724–20727.

(25) Rudd, P. A.; Liu, S.; Planas, N.; Bill, E.; Gagliardi, L.; Lu, C. C. *Angew Chem Int Edit* **2013**, *52*, 4449–4452.

(26) Clouston, L. J.; Siedschlag, R. B.; Rudd, P. A.; Planas, N.; Hu, S.; Miller, A. D.; Gagliardi, L.; Lu, C. C. *J Am Chem Soc* **2013**, 130823151958007.

(27) Cantat, T.; Scott, B. L.; Kiplinger, J. L. *Chemical Communications* **2010**, *46*, 919–921.

(28) Kiplinger, J. L.; Morris, D. E.; Scott, B. L.; Burns, C. J. *Organometallics* **2002**, *21*, 5978–5982.

(29) Shannon, R. D. *Acta Crystallographica Section A: Crystal Physics* **1976**, *32*, 751–767.

(30) Scott, J.; Basuli, F.; Fout, A. R.; Huffman, J. C.; Mindiola, D. J. *Angew. Chem. Int. Ed. Engl.* **2008**, *47*, 8502–8505.

(31) Cantat, T.; Graves, C. R.; Scott, B. L.; Kiplinger, J. L. *Angew Chem Int Edit* **2009**, *48*, 3681–3684.

(32) 217–240.

(33) Meyer, T. J.; Caspar, J. V. *Chem Rev* **1985**, *85*, 187–218.

(34) Gardner, B. M.; Lewis, W.; Blake, A. J.; Liddle, S. T. *Inorg Chem* **2011**, *50*, 9631–9641.

(35) Arnold, P. L.; Mansell, S. M.; Maron, L.; McKay, D. **2012**, 1–7.

(36) Jansen, G.; Schubart, M.; Findeis, B.; Gade, L. H.; Scowen, I. J.; McPartlin, M. *J Am Chem Soc* **1998**, *120*, 7239–7251.

(37) Tilley, T. D.; Andersen, R. A. *J. Chem. Soc., Chem. Commun.* **1981**, 985.

(38) Bentsen, J. G.; Wrighton, M. S. *J Am Chem Soc* **1987**, *109*, 4530–4544.

(39) Job, R. C.; Curtis, M. D. *Inorg Chem* **1973**, *12*, 2514–2519.
(40) Triplett, K.; Curtis, M. D. *Inorg Chem* **1976**, *15*, 431–433.
(41) Knox, S. A. R.; Stone, F. G. A. *J. Chem. Soc., A* **1971**, 2874.
(42) Addison, A. W.; Rao, T. N.; Reedijk, J.; van Rijn, J.; Verschoor, G. C. *J Chem Soc Dalton* **1984**, 1349.
(43) Pyykkö, P.; Atsumi, M. *Chem-Eur J* **2009**, *15*, 186–197.
(44) Mills, D. P.; Moro, F.; Mcmaster, J.; van Slageren, J.; Lewis, W.; Blake, A. J.; Liddle, S. T. *Nature Chem* **2011**.
(45) Werle, C.; BAILLY, C.; Karmazin-Brelot, L.; Le Goff, X.-F.; Ricard, L.; Djukic, J.-P. *J Am Chem Soc* **2013**, 131101105733004.
(46) Bungu, P. N.; Otto, S. *Dalton T* **2011**, *40*, 9238.
(47) Edgell, W. F.; Lyford, J., IV. *Inorg Chem* **1970**, *9*, 1932–1933.
(48) SMART: Area Detector Software Package Bruker Analytic X-ray Systems I. Madison WI, **2003**.
(49) SADABS: Bruker-Nonius Area Detector Scaling and Absorption V2.05 Bruker Analytical X-ray System I. Madison WI, **2003**.
(50) G. M. Sheldrick, *Acta. Crystallogr. A.* **2008**, *64*, 112.
(51) L. J. Farrugia, *Appl. Crystallogr.* **1997**, *30*, 565.
(52) P. van der Sluis, A. L. Spek, *Acta Cryst.* **1990**, *A46*, 194.

Insert Table of Contents artwork here

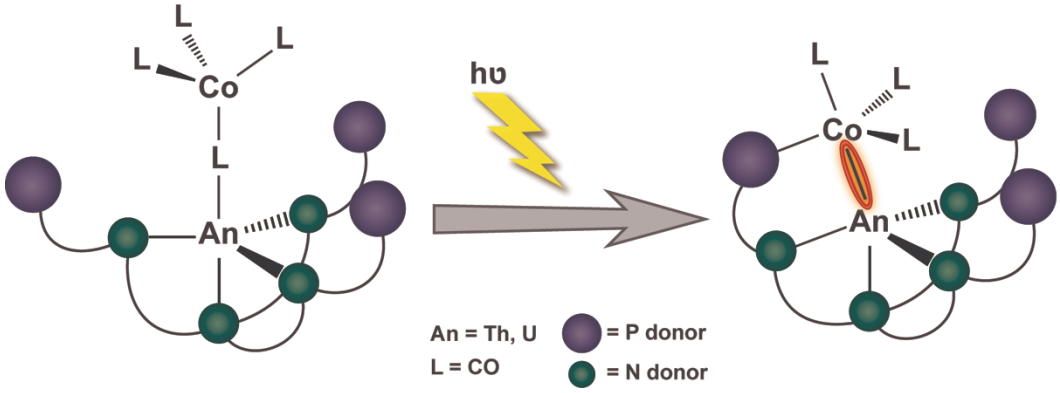

DISCLAIMER